J. Biomedical Science and Engineering, 2015, 8, 170-183
Published Online March 2015 in SciRes. http://www.scirp.org/journal/jbise
http://dx.doi.org/10.4236/jbise.2015.83017

Reliability and Precision Are Optimal for Non-Uniform Distributions of Presynaptic Release Probability

Jean-Marc Fellous[1,2*], Nadia S. Corral-Frías[1]

[1]Graduate Interdisciplinary Program in Neuroscience, University of Arizona, Tucson, USA
[2]Department of Psychology and Applied Mathematics, University of Arizona, Tucson, USA
Email: [*]fellous@email.arizona.edu

Received 27 December 2014; accepted 12 March 2015; published 19 March 2015

Copyright © 2015 by authors and Scientific Research Publishing Inc.
This work is licensed under the Creative Commons Attribution International License (CC BY).
http://creativecommons.org/licenses/by/4.0/
Open Access

Abstract

Most conceptual and computational models assume that synaptic transmission is reliable, a simplification rarely substantiated by data. The functional consequences of the recruitment of high and low initial release probability synapses on the reliability and precision of their postsynaptic targets are studied in a multi-compartmental model of a hippocampal CA1 pyramidal cell. We show that changes in the firing rate of CA3 afferent inputs (rate remapping) are not reflected in the firing rate of the CA1 cell but in the reliability and precise timing of some of its action potentials, suggesting that a signature of remapping may be found in the precise spike timing of CA1. Our results suggest that about half of the action potentials produced by a CA1 cell can potentially carry reliable information in their precise timing with about 25 ms precision, a time scale on the order of the gamma cycle. We show further that reliable events were primarily elicited by CA3 synapses in a state of low probability of release. Overall, our results suggest that the non-uniform distribution of initial release probabilities observed experimentally achieves an optimum yielding simultaneously high precision and high reliability, and allows large populations of CA3 synapses to contribute to the production of reliable CA1 spiking events.

Keywords

Spike Timing, Hippocampus, Computational Model, Synapses

1. Introduction

In vivo, hippocampal and cortical cells receive a large amount of background subthreshold synaptic inputs in

[*]Corresponding author.

How to cite this paper: Fellous, J.-M. and Corral-Frías, N.S. (2015) Reliability and Precision Are Optimal for Non-Uniform Distributions of Presynaptic Release Probability. *J. Biomedical Science and Engineering*, **8**, 170-183.
http://dx.doi.org/10.4236/jbise.2015.83017

addition to information rich inputs to which they respond by emitting action potentials. CA1 pyramidal cells are well known to contribute to a precise code for spatial location. Several lines of experimental evidence suggest that the precise generation of action potentials in the hippocampal region CA1 may have functional significance.

Studies *in vitro* suggest that the precise timing (10 - 20 ms) of pre and post synaptic activation may result in long-term increases or decreases in synaptic strength [1] [2]. Precise and reliable firing can be achieved *in vitro* by current injection at the soma [3] and is highly dependent on the frequency content of the stimulus [4]. There is evidence *in vivo* that information about the position of an animal within a CA1 place field might be carried by the precise timing of action potential generation with respect to theta oscillations, a phenomenon termed phase precession [5]. For a CA3 or CA1 place cell to phase-precess, the firing displacement from cycle to cycle should be tightly controlled within temporal windows on the order of 10 - 20 ms. Finally, it has been shown that pyramidal cells in hippocampus or cortex can precisely fire relative to each other during periods of reactivation in sleep or quiet wakefulness [6]-[8], again on time scales of a few tens of milliseconds.

Several theories have been proposed to explain how reliability and precision emerge from presynaptic correlations or strong synapses [9] [10]. Only a few of these theories take into account the stochastic and highly dynamical nature of the synaptic probability of release and its heterogeneity among synapses impinging upon the same cell [11] [12]. How this probability of release and its short term dynamics allow for the reliable and precise generation of action potentials in the face of large amounts of background noise is still poorly understood. One possibility is that reliable firing events occur if the average probability of release of background information-poor and signal information-rich synapses is different.

To study the conditions in which stochastic synaptic transmission allows for the generation of reliable and precise spikes trains, we use the well-studied CA3-CA1 pathway where the biophysical details of synaptic transmission, synaptic integration and action potential generation are well understood and quantified. In this system, CA3 Schaffer collateral synapses (CA3 to CA1 axons in the stratum radiatum) have an average release probability on the order of 25% [13] [14] and exhibit a non-uniform distribution of initial probability of release, with some synapses significantly more reliable than others [13]-[16]. We built a multi-compartmental biophysical model of a reconstructed CA1 pyramidal cell contacted by CA3 AMPA/NMDA stochastic synapses that included facilitation and depression. We investigated the functional consequences of the recruitment of high and low initial release probability CA3 synapses on the reliability and precision of CA1 pyramidal cells.

2. Materials and Methods

All simulations were performed using the NEURON simulator [17] with a time step of 0.1 ms. Data analyses were conducted in Matlab using custom written software.

2.1. Cell Morphology

To illustrate the consequence of recruiting high or low probability synapses on the output of a cell, we use a simplified single compartment model (**Figure 1**). This "ball neuron" contains all the currents of the multi-compartment cell, tuned so that input resistance and membrane potential are within 5% of that of the multi-compartment cell. We then used a reconstructed multi-compartmental CA1 cell from the Duke/Southampton cell archive (cell n180). This cell was chosen to represent the typical cell population available in terms of surface area and branching structure (cells n400 and n123 were also studied, but are not discussed here for simplicity). The cell membrane area was 74,686 μm^2, and contained about 600 compartments (**Figure 2(b)**). The cell surface was corrected to account for spines [18]. Further details are given in Supporting Information.

2.2. Cell Physiology

The dendritic compartments were devoid of active currents, except for their aggregate influence on the membrane potential near rest (sigmoid leak conductance). This modeling choice was motivated by the desire to stay simple and independent from particular assumptions on the nature and densities of the many currents known to be present in dendrites [19], and by the finding that in spite of all these currents, the synaptic summation in CA1 dendritic trees was essentially linear [20]. Also, most of the simulations were performed with small numbers of synapses, under conditions where spontaneous background synaptic activity was minimal. In these conditions, the dendritic membrane potential was presumably undergoing small fluctuations near rest, and hence

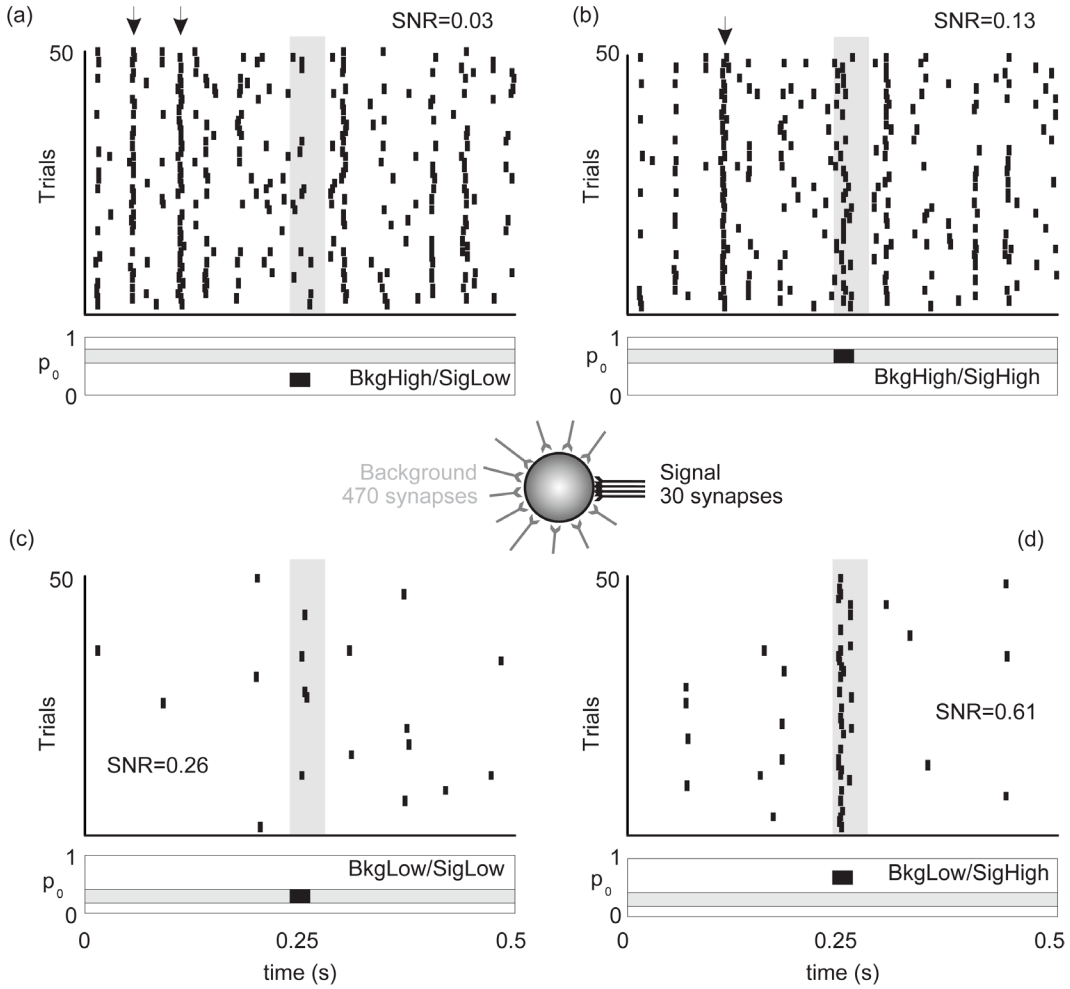

Figure 1. Response (50 trials) of a simplified model neuron to a signal embedded in background noise. The signal is carried by 30/500 AMPA/NMDA synapses (inset). The initial probability of release (p_0) of all Background or all Signal inputs are set at two levels (Low: p_0 = 0.28, High: p_0 = 0.65) and the four combinations of Background/Signal probability of release are shown in the four panels and graphically depicted under each rastergram. (a) Background-High, Signal-Low; (b) Background-High, Signal-High; (c) Background-Low, Signal-Low; (d) Background-Low, Signal-High. In all panels the signal-to-noise (SNR) ratio is indicated and the gray areas mark the time interval when the response of the cell is expected and where the SNR is computed.

was unlikely to trigger significant active voltage-dependent excursions beyond those captured by the non-uniform leak conductance. Further work would be needed to assess the role of specific dendritic current combinations [21]. Quantitative details on the cell physiology parameters are given in Supporting Information.

As will be described below, the model of the synapse was tuned on the basis of *in vitro* experimental work. Our simulations, however, aim at explaining *in vivo* phenomena. We assume that synaptic releases dynamics are similar *in vivo* and *in vitro*, but we adjust the intrinsic parameters of the CA1 cells to what is known from *in vivo* experiments. Details on these adjustments are given in Supporting Information.

2.3. Synaptic Physiology

2.3.1. Time Scale Limitations

In CA1, excitatory synapses exhibit short term facilitation and depression that are mainly the result of short term changes in the probability of release. These changes can occur at time scales in the range of 8 - 25 ms [15] [22]. At these time scales the effects of facilitation and depression are highly variable at individual synapses and a

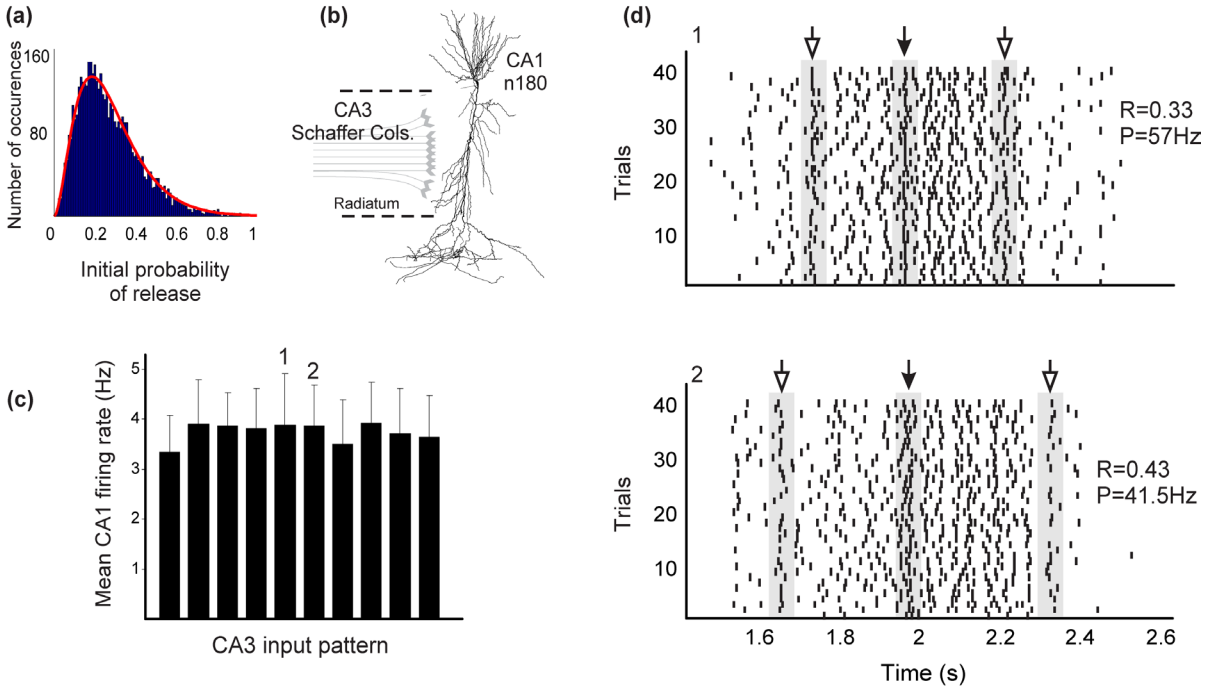

Figure 2. (a) Distribution of initial release probability of 5000 model synapses (see methods). The red curve shows the gamma curve obtained experimentally [35]; (b) Reconstructed CA1 multi-compartmental cell used in this study (Duke/Southampton cell archive, n180). Dashed lines indicate the sections of the dendritic tree where CA3 synapses were distributed; (c) CA1 mean in-field firing rate for 10 random distributions (remappings) of CA3 presynaptic spike times on 500 synapses. Synapse locations are identical. Presynaptic CA3 spike times were taken from the experimental data of Leutgeb *et al*. 2004. There are no significant differences in firing rates between any two of the 10 firing rates. $P > 0.05$ for all pairs (student t-tests); (d) Sample rastergrams from two of the remappings 1 and 2 in C showing that while firing rates are nearly identical, precise spike timing events spontaneously emerge in the course of the simulations. Closed arrows: reliable spike time event common to the two remappings, open arrows reliable spike time events specific to each remappings. Reliability (R) and Precision (P) are indicated for each rastergram (see methods).

clear understanding of the underlying mechanism is yet to be achieved. At time scales larger than 40 ms, consistent data on facilitation and depression can be found in the hippocampus [13] [23]. Synaptic dynamics also change on the time scales of seconds to minutes. Post-tetanic potentiation, augmentation and other long term effects (LTP and LTD) have been extensively studied, and may be of importance for long lasting phenomena such as those implicated in learning, or for conditions where long presynaptic spike trains are evoked. Because we focus on neural activity that last at most 2 or 3 seconds and involve short spike trains (2 - 20 spikes, traversal of a place field), we restrict our model to synaptic dynamics that have time constants in the 40 ms - 2 sec time range. Note also that in choosing specific sets of *in vitro* experimental data to tune our model, care was taken to only use experimental conditions that are compatible, especially when pertaining to extracellular concentrations of calcium and magnesium.

2.3.2. Modeling Assumptions and Choices

The dynamic stochastic synapse we used was based on previous experiments using minimal stimulation and inspired by other theoretical formulations [24] [25]. The model assumes that at most one vesicle is released per presynaptic action potential [26] [27], and that if one afferent axon makes multiple synapses on the same postsynaptic target, these synapses are independent.

As for all models, a balance needs to be stricken between complexity (biophysical realism) and explanatory power. In designing the model, we opted for a formulation in which facilitation and depression are two independent entities, each with their own time constant and magnitude (4 parameters), that can be fully constrained by physiological data. Furthermore, because experimental evidence suggested that the heterogeneity of synaptic dynamics in CA1 glutamatergic synapses was related to initial release probability, we made this probability an

explicit variable [28]. We did not explicitly model synaptic calcium dynamics, which is an important factor underlying these two forms of short term plasticity [29]-[31] partly because our emphasis is on single synapse stochasticity and because data on calcium dynamics are mainly applicable to phenomenological (average) models. However, we show below that after proper parameter adjustment, this model gave good fits to data that were not used to tune it.

Most of the experimental data gathered on synaptic transmission *in vitro* was obtained at room temperature (e.g. [13] [15] [32]). Accordingly, we built, tuned and validated our model of synaptic transmission using datasets obtained at room temperature from different laboratories. We note that some differences in tuning may result if the temperature is raised to physiological levels [33]. We did not find sufficient published data obtained at physiological temperatures to simultaneously tune and validate our model, especially using the minimal stimulation technique. We however compensated for the temperature discrepancy by adjusting the physiological characteristics of CA1 firing to mimic that obtained *in vivo* in the anesthetized animal (see "cell physiology" above).

Finally, because we intend to make quantitative predictions about the relationship between the stochasticity of Schaffer collateral synapses and the firing of CA1 pyramidal cells, we use different datasets from different laboratories to separately adjust and validate the model parameters. Validation is taken here to mean the generation of predictions that have been confirmed experimentally in studies and protocols that have not been used to adjust the model.

2.4. Model of Stochastic Release

The probability of release of a single synapse was given by the equation

$$P_r(t) = 1 - e^{-F(t)/D(t)} \tag{1}$$

where F and D are time-dependent variables representing facilitation and depression, respectively. At each excitatory synapse, when a presynaptic spike is received at time t, a random number from a uniform distribution is drawn and the probability of release, $P_r(t)$, is calculated based on the current release history S (the subset of presynaptic spike times at which the synapse has indeed released). If the random number is larger than $P_r(t)$, a postsynaptic potential is generated, and S is updated. Note that it is not necessary to update $P_r(t)$ for each synapse at every simulation time increment but only when a presynaptic spike occurs at that synapse.

Each individual synapse had five parameters: The unitary conductance, the initial amount of facilitation and depression (F_0 and D_0 respectively), the amount of facilitation produced by a single presynaptic action potential (F_{mag}), and the amount of depression resulting from a single release (D_{mag}). Details on the explicit formulations for $F(t)$ and $D(t)$, and on the tuning of their parameters are given in Supporting Information.

2.5. Distribution of Initial Release Probabilities

The initial release probability (p_0) is not uniform across hippocampal synapses in the same CA1 pyramidal cell (**Figure 2(b)** shows the cell used in this study), as well as on average across many such cells [22] [34]-[36]. The distribution is well described by a gamma function of the form:

$$N(p_0) = {p_0}^2 e^{-\lambda p_0} \tag{2}$$

where $N(p_0)$ is the number of synapses with initial probability p_0, and λ (here $\lambda = 10.7$) is a constant such that the average probability across all synapses of this distribution is about 0.28 [35]. With $D_0 = 1$ by convention, $F_0 = -\log(1 - p_0)$ and the distribution of F_0 is completely defined by the distribution of initial release probabilities p_0.

Figure 2(a) shows the distribution of initial release probabilities resulting from the random draw of 5000 F_0 values constrained by p_0 as described above, together with the fit given by experimental data [35].

2.6. Postsynaptic Synaptic Currents

Excitation: The dynamics of the postsynaptic AMPA current was obtained upon release using a two state kinetic scheme, NMDA channels were similarly modeled with 5 states, including desensitization and re-sensitization [37].

Inhibition: The simulations conducted here used real CA3 spike trains recorded *in vivo* while animals traversed a place field. Inhibitory cells in the cell body layer typically do not show place specificity [38], and in the time course of the traversal can be considered tonically active. Due to the complexity of the inhibitory cell population and the lack of detailed data on GABAergic synaptic transmission (e.g. depression, facilitation), we opted for a simplified implementation of feed forward inhibition. Inhibition was represented by an Ornstein-Uhenbeck process inserted in all compartments of the soma, as in previous work [39] [40].

Details on the tuning of the synaptic conductances and their validation are given in Supporting Information.

2.7. Input Spike Trains

In order to provide our model with realistic inputs, we use data provided by S. Leutgeb and published elsewhere [41]. The inputs spike trains to our model CA1 cells were taken from a population of 37 CA3 pyramidal cells recorded simultaneously in four 10 minutes sessions, as the animal was exploring a rectangular box [41]. In most simulations we chose random sets of 500 of these real spike trains to simulate a realistic CA1 input. Details on the input spike trains, and justification for this number of spike trains are given in Supporting Information.

2.8. Reliability and Precision

In order to assess the extent to which the response of a CA1 cell is reliable, we repeat all simulations 40 times, with the same presynaptic CA3 spike trains, but with different seeds for the stochasticity of the synapses. It is unlikely that, *in vivo*, the exact same presynaptic pattern of activation reoccurs, so these simulations are not meant to represent a realistic case. The goal of these repeated stimulations is to identify which spikes (if any) of the CA1 cell are potentially specific to the presynaptic pattern of activation, and therefore potential carrier of information about the input. These CA1 spikes would be re-emitted more often than chance during the 40 presentations. Other spikes would not. These reliable patterns of spiking are visually detectable as alignments in the rastergram of the CA1 response across the 40 trials ("Events", **Figure 3** arrows). To quantify their occurrence we use the "direct method" for the computation of reliability and precision [10]. Details on these computations are given in Supporting Information.

3. Results

To investigate how the short term dynamics of the probability of release allow for the reliable and precise generation of action potentials, we first used the simplified biophysical ball neuron (**Figure 1**, center inset, see methods for details). The simulations show that the worst Signal-to-Noise Ratio (SNR) is achieved when background synapses have high release probability and signal synapses have low release probability (Panel A, BkgHigh/SigLow, SNR

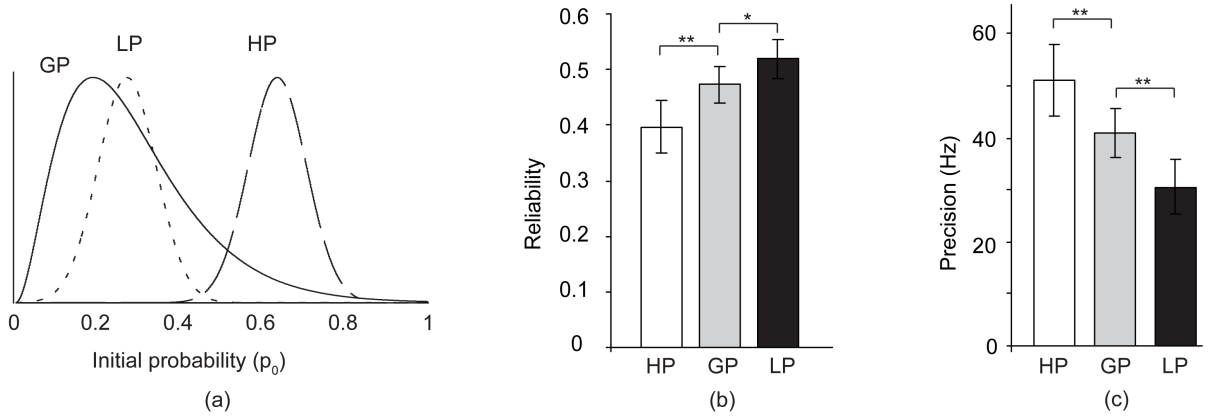

Figure 3. Reliability and precision for three different distributions of initial probability of release. (a) GP is the Gamma distribution obtained experimentally (**Figure 1(b)**), LP is a Gaussian distribution of the same mean as GP but not including high probability synapses (tail of GP), HP is a Gaussian distribution of mean 0.65 which does not include low probability synapses; (b) Reliability; (c) Precision. All simulations results were obtained with 500 synapses. Each bar is obtained on the basis of 15 different presynaptic spike patterns obtained from the CA3 data (see methods and supplemental information), repeated 40 times. $^{*}p < 0.05$, $^{**}p < 0.01$ (student t-tests).

= 0.03). Note the emergence of spurious reliable events as alignments across multiple trials (arrows). These events are due to the random occurrence of nearly synchronous spike times in several background synapses (the synapses responsible for the different events are not necessarily identical). If the probability of signal synapses is raised to the same level as that of the background, the cell emits a reliable event at the appropriate time (**Figure 1(b)**, gray box), but several others at unwanted times, yielding a low SNR (Panel B, BkgHigh/SigLow, SNR = 0.13). If both background and signal synapses are low, very few spikes are emitted, the cell is unresponsive except on a very few trials and the SNR is again low (Panel C, BkgLow/SigLow, SNR = 0.26). The best SNR is obtained when the background probability of release is low and the signal probability of release is high (Panel D, BkgLow/SigHigh, SNR = 0.61). These results suggest that for precisely and reliably timed events to be produced in a population of synapses of identical potency (same somatic EPSC size), the information has to be selectively routed on synapses with high release probability. This result is puzzling on three accounts: First it is difficult to imagine how such a specific synapse selection might occur dynamically, accounting for dendritic filtering and for the highly variable process of information transmission. Second, the population of high probability synapses, at least in the hippocampus CA3-CA1 pathway, is very small, severely limiting the amount of "signal" channels available (**Figure 2(a)**). Third, the synaptic probability of release is a highly dynamical variable that changes on the times scale of milliseconds as synapses undergo depression and facilitation, so that signal transmission should be appropriately timed to reach the synapse when its probability of release is high.

3.1. Spike Rate vs. Spike Timing

The CA3-CA1 pathway was used to study the conditions in which stochastic synaptic transmission allow for the generation of reliable and precise spikes trains. We assessed the response of a reconstructed CA1 cell to inputs representing the traversal of a place field. To ensure that the pattern of presynaptic inputs was as close as possible to *in vivo* data, the inputs spike trains to the model cell were taken from a population of 37 CA3 pyramidal cells recorded simultaneously in four 10 minutes sessions, as a rodent explored a rectangular box [41]. For each cell, place fields were characterized using video tracking data (single place fields, all data kindly provided by Dr. S. Leutgeb). Each traversal of each place field of each cell was isolated, and the corresponding spike trains were collected (992 spike trains, mean in field discharge was 4.7 Hz range 0.1 - 20 Hz, see supplemental material).

Figure 2(c) shows the firing rate variability of the CA1 cell across 10 different sets of presynaptic CA3 spike trains. Each spike train was randomly assigned to one of 500 synapses distributed randomly in the compartments of the CA1 cell within the stratum radiatum area. Forty trials per presynaptic spike time set were simulated (error bars). The 10 redistributions of presynaptic spike trains simulated 10 different rate remappings in CA3 [42]. No significant difference in CA1 firing rate were detected across any of the conditions (paired t-tests $p > 0.1$), suggesting that CA3 rate remapping cannot yield CA1 rate remapping through the type of stochastic synapses used here, consistent with experimental data [43]. We further used these 40 trials to assess the extent to which timing information may be present as "events" across trials. If indeed a subset of CA1 action potentials are a consequence of some specific aspects of the CA3 presynaptic inputs (e.g. synapse locations, pattern of presynaptic spike times, synapse initial release probability), then some of the CA1 spikes should occur reliably across multiple trials ran with identical CA3 presynaptic input patterns. Panel 2D shows the rastergrams resulting from two of the remappings shown in Panel A (1 and 2). It is clear from these simulations that, even though the CA1 cell firing rates are not different across the 40 trials, timing information is present (arrows), and some reliable spike times emerge, as with our simple model (**Figure 1(a)**, **Figure 1(b)**, **Figure 1(d)**). Some reliable spike times are common to the two rate remappings (dark arrows, Panel 2D), others are specific to the pattern of CA3 presynaptic times being used (open arrows, Panel 2D). This result suggests and predicts that while rate remapping in CA3 may not be reflected in the firing rate of a specific CA1 cell, some signature of the remapping may be found in its precise spike timing.

Since the nature of the "signal" and "background" is unknown, we used measures of reliability and precision to quantify the emergence patterns of spike times rather than SNR ([10] and see methods). Reliability measures the consistency of firing at specific times from trial to trial ($0 < R < 1$, 1 very reliable) and precision is inversely proportional to the average jitter of firing around reliable spike times (expressed in Hz, high frequency is high precision). The rastergrams in **Figure 2(d)** had a reliability and precision of 0.33 and 57 Hz (1, top) and 0.43 and 41.5 Hz (2, bottom) respectively. The mean reliability and precision for all the remapping simulations in **Figure 2(c)** were 0.47 ± 0.1 and 40 ± 15 Hz respectively. Almost half (47%) of all spikes belonged to events

(alignments across trials, as in arrows in **Figure 2(d)**) and the average temporal jitter of these alignment was 25 ms. These results suggest that about half of the spikes produced by the modeled CA1 can potentially carry reliable information in their precise timing within 25 ms precision, a time scale on the order of the gamma cycle.

3.2. Contribution of High and Low Probability Synapses to Precision and Reliability

In this model, the variability of the CA1 response is due to the stochasticity of the synapses. Unlike most models, and compatible with experimental data, synapses here have different initial release probabilities distributed along a tailed gamma-like distribution function (**Figure 2(a)**). In this distribution, most synapses have a low probability of release (around 0.28), and a few synapses have a high release probability (above 0.5). In order to assess the extent to which reliability and precision depend on initial release probability, we repeated the simulations above using a Gaussian distribution of low initial probabilities (0.28, **Figure 3(a)**, dotted line, LP) which did not include any high probability synapse, a gamma distribution as observed experimentally (**Figure 3(a)**, continuous line, GP) and a Gaussian distribution with higher mean (0.65, **Figure 3(a)**, dashed line, HP), which did not include low probability synapses. The conductances of all synapses were equal and adjusted so that the average firing rate of the CA1 cell was identical in the three conditions (about 3.5 Hz, as in the data, see supplemental methods). Perhaps counter-intuitively, the reliability of the CA1 response was lowest in the case of the Gaussian with high mean initial release probability (white bars HP), and highest in the case of the Gaussian distribution with the lowest initial release probabilities (LP) (**Figure 3(b)**). This result may stem from the fact that high probability synapses make the CA1 cell more sensitive to non-synchronous presynaptic inputs. Such spikes occur outside events, and hence decrease the reliability. On the other hand, low probability synapses only allow the CA1 cell to fire when it receives a sufficiently synchronous presynaptic input volley. The results presented here suggest that if a neural code uses synchrony as a way of conveying information, too many high probability synapse would make the CA1 cell sensitive to noise (*i.e*. non synchronous inputs), while low probability synapses would make the cell sensitive to the "signal" (*i.e*. synchronous inputs). **Figure 3(c)** also shows the precision for these three release probability distributions. Precision is highest for the HP distribution, and lowest for the LP distribution. The Gamma distribution (GP) therefore achieves a compromise between high and low values for both precision and reliability. This result is compatible with the results shown in the simple model (**Figure 1(d)**, BkgLow/SigHigh) in which the SNR is the highest, and in which the distribution of presynaptic release probability is double peaked with the majority of synapses having low probability, and a few having high probability. In the CA1 simulation however, synaptic dynamics are such that the release probability of a synapse at the time of an event is not necessarily high, as in **Figure 1(d)**.

In order to determine which synapses are responsible for events, we plotted the presynaptic CA3 spike trains around a representative CA1 event (**Figure 4**). This plot allows for the global visualization of when CA3 spikes were received at which synapses, just before the CA1 cell fired reliably (firing of CA1 is not shown for clarity, the time of reliable firing is indicated by the vertical red line). **Figure 4(a)** shows the CA3 spike trains for all 500 synapses, 100 ms around the time of occurrence of a CA1 event (vertical red line). In this plot, the initial probability of release is pulled from a Gaussian distribution of mean 0.28 (LP, black bars in 3B, C). The inset shows the distribution of initial probabilities. The synapses are sorted in increasing order of release probability at the time of the event, so that synapse #0 had the lowest release probability at the time marked by the vertical red line (here, $p = 0.02$), and synapse #500 had the highest probability of release (here, $p = 0.77$). This graph demonstrates that two distinct populations of synapses were involved in the triggering of this event: a small group of synapses in a state of low release probability (100 synapses, between indices 0 and 100, bottom grey box), and a group of synapses in a state of high probability (50 synapses between indices 450 and 500, top grey box). The other 350 synapses did not receive a significant number of presynaptic spikes and therefore did not contribute to the spiking at that specific event. This distribution of probability is similar to that of **Figure 1(d)** (BkgLow/SigHigh), even though all synapses started with low initial release probabilities (0.28, as in 1C, BkgLow/SigLow). This result shows that the synaptic population self-organizes into an optimal (*i.e*. highest SNR) distribution of release probability and dynamically transitions from a BkgLow/SigLow type composition to a BkgLow/SigHigh composition prior to a reliable event. Only a small fraction of synapses (150/500) actually contribute to each reliable event.

Figure 4(b) shows the presynaptic spike trains responsible for an event, when the initial probabilities of release were obtained from a Gaussian distribution of mean 0.65 (HP, white bars in **Figure 3(b)**, **Figure 3(c)**). In

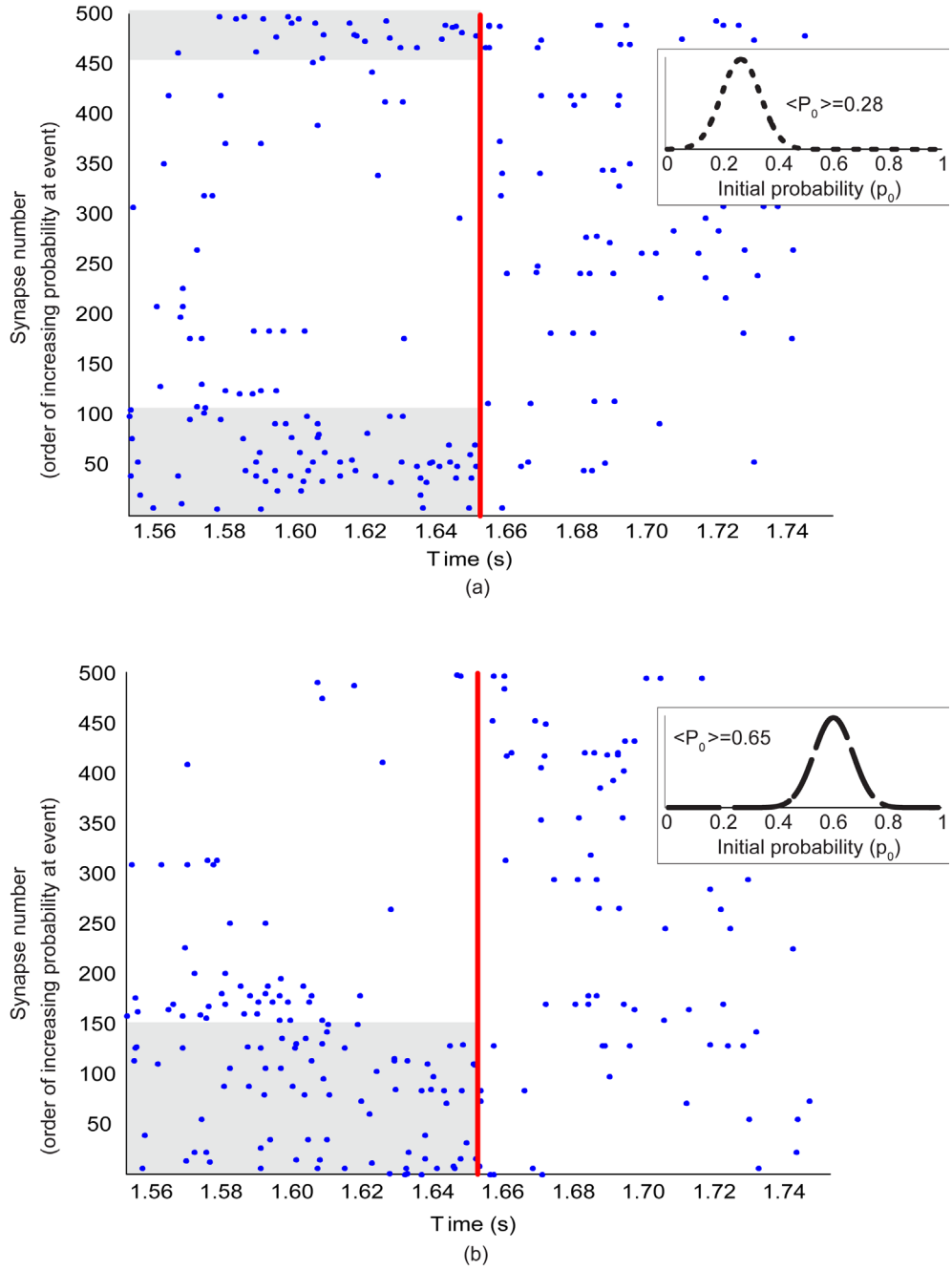

Figure 4. Presynaptic CA3 firing patterns before a representative CA1 event in the cases of synapses with initial probability of releases that are distributed as a Gaussian around 0.28 (a) and Gaussian around 0.65 (b). Synapses are ordered according to their instantaneous probability of release at the time of the event (red vertical line). Index 0 corresponds to the lowest probability. Insets are as in **Figure 3(a)**. Grey boxes highlight the synapses and presynaptic spikes contributing to the event.

this case, the population of synapses that was responsible for this CA1 event is single-peaked and includes synapses in a state of low probability of release at the time of the reliable event (150 synapses, numbered between 0 to about 150, grey box), even though all synapses had initially a strong release probability (as in **Figure 1(b)**, BkgHigh/SigHigh). At the time of the event, however, all synapses were strongly depressed. This result is analogous to that of **Figure 1(c)**—BkgLow/SigLow, in that if an event occurs, its reliability is low but it is precise (**Figure 3(b)**, **Figure 3(c)**, HP). These results show that the population of synapses dynamically transitions from

a population of type BkgHigh/SigLow (**Figure 1(b)**) to that of type BkgLow/SigLow (**Figure 1(c)**) just before an event. Again, only a small fraction of synapses (150/500) contribute to the event. Interestingly, the transition does not evolve further to type BkgLow/SigHigh (**Figure 1(d)**) as would be expected from the results of **Figure 4(a)**, keeping the events precise but low reliability.

To quantify these observations, we collected simulation results across events, and across different presynaptic distributions (*i.e*., 10 rate remappings). In these simulations the membrane time constant of the CA1 cell was 24 ms, and the lowest event precision was about 40 Hz (*i.e*. jitter of 25 ms). This suggests that CA1 spiking is likely due to presynaptic CA3 inputs arriving less than 50 ms before a CA1 spike. We plotted the average number of spikes occurring 50 ms before an event at each of the 500 synapses for the low probability distribution (LP; 47 events, **Figure 5(a)**). The average number of spikes received at a synapse within these 50 ms represents a measure of the contribution of a particular synapse to an event. The plot shows two peaks at synapses with low (P_{re} ~ 0, inset) and high (P_{re} ~ 0.4, inset) release probabilities at the time of the event. The inset shows that the overall distribution of release probability of all synapses at the time of the events was Gaussian-like, centered on low release probabilities (0.15). This suggests that at the time of events all synapses were strongly depressed. **Figure 5(b)** shows that a high initial release probability distribution HP (51 events) leads to a smoothly decaying distribution of presynaptic spikes where synapses with low release probabilities received more presynaptic spikes than synapses with higher release probability. The inset shows that the distribution of release probabilities at the time of events was approximately uniform, but limited to low releases (P_{re} ~ <0.4). Although all synapses had high initial release probabilities (HP is centered at 0.65), almost all synapses were depressed and contributed equally to the events. This group data confirms the conclusions reached on the basis of the representative example shown in **Figure 4** and further indicates that unlike in **Figure 1**, reliable events were primarily elicited by synapses in a state of low probability of release.

The Gamma distribution of initial release probabilities observed experimentally allows for a tradeoff between high reliability and high precision (**Figure 3(b)**, **Figure 3(c)**, gray bars, GP), recruiting BkgLow/SigHigh probability synapses (**Figure 1(d)**) which would be optimal if the events were only triggered by high probability synapses. However, the analysis of the synapses contributing to an event (**Figure 5(c)**) performed here reveals a more homogeneous recruitment. The synapses responsible for events are in various states of release probability, with a bias for lower probabilities. **Figure 5(d)** shows the distribution across 10 CA3 rate re-mappings. The distribution is significantly more uniform than in panels A and B, with a slight bias for probabilities in the lowest 20% range (P_{re} < 0.15). This distribution contains an approximately equal number of spikes received by synapses with release probabilities between 0.15 and 0.95 at the time of the events. The inset shows that the overall distributions of probabilities at the time of the events was gamma-like (peak P_{re} = 0.12) with a few synapses with strong release probability (P_{re} > 0.5).

These results show that both low and high initial release probability synapses are required for the generation of events that are both reliable and precise. If high probability synapses are eliminated (LP), precision decreases and reliability increases. Events occur in response to the recruitment of depressed synapses with release probabilities on either flank of a Gaussian distribution. If low probability synapses are eliminated, reliability decreases (HP), but precision increases. Events occur in response to the recruitment of synapses in various states of low probability of release. The gamma-shaped distribution of initial probability of release (GP) realizes a tradeoff between reliability and precision. In that case, events occur in response to the uniform recruitment of most synapses.

4. Discussion

Overall, the results shown here suggest that the variability of CA1 cell responses observed *in vivo* during place field traversals [44] is at least in part due to the stochasticity and short term dynamics of Schaffer collateral synapses. In general, short term synaptic dynamics and spike-history dependence may have functional consequences. They can act as frequency filters [12], presynaptic spike patterns detectors [45] controllers of the input-output gain of individual cells [46] [47], sources of bistability [48], and in general, increase the computational power of neural networks [24] [25] [49]. Previous work has shown that an increase in the amount of information transmitted is possible through the elimination of presynaptic spike train redundancies, using depressing synapses [50] [51]. These studies, and most conceptual and computational models, assume that the stochasticity of CA3 to CA1 synapses is uniform. Our results suggest that these models may need to be re-evaluated in the light of the heterogeneity of synaptic transmission.

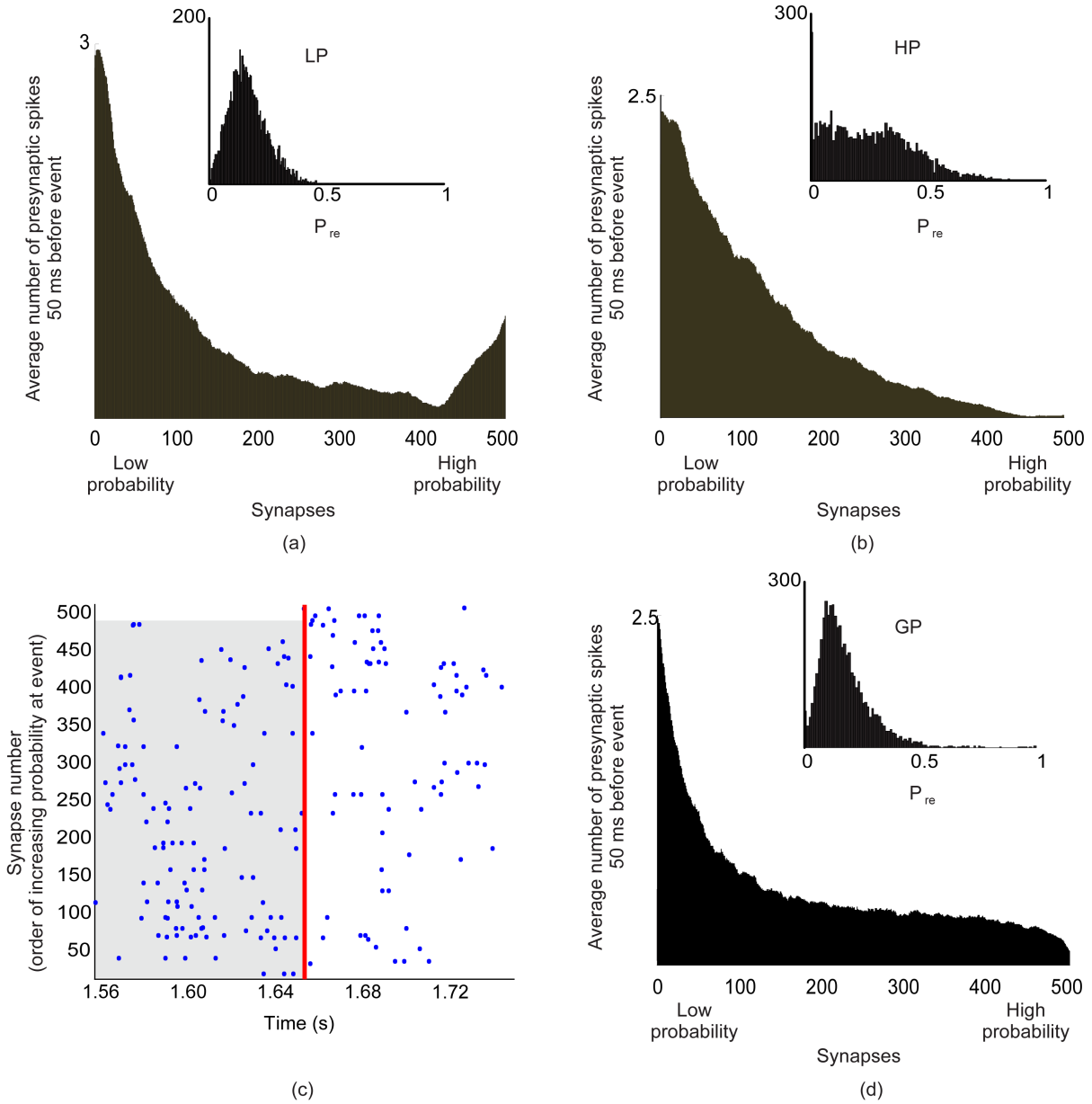

Figure 5. Average number of presynaptic spikes before an event for initial probability of releases distributed as a Gaussian centered at 0.28 (a), centered at 0.65 (b) and for the gamma distribution (d). (c) Representative presynaptic pattern around an event for the Gamma distribution GP. Panels A, B and D were each obtained for 500 synapses stimulated by 10 presynaptic patterns 40 times. Synapses are ordered by their instantaneous probability of release at the time of each event. The distributions in Panels A, B and D are obtained by subtracting the analogous distributions computed for random (non-aligned) events.

Before place field traversal, CA3 cells are essentially silent, therefore, when entering the place field, the CA3-CA1 synapses will release according to their initial release probability. Since different synapses have different initial probabilities of release [22] [34]-[36], their patterns of release, and therefore their contribution to postsynaptic firing, are likely to be significantly different during the course of place field traversal. Our model predicts that the gamma-like shape of the initial release probability distribution achieved an optimum such that, in principle, all synapses could contribute to the reliable spiking of the CA1 cell. Gaussian distributions resulted in a *de facto* selection of sub populations of synapses, leaving a significant portion of synapses unlikely to contribute to reliable CA1 firing. Our results demonstrate therefore that the gamma-shaped distribution of initial release

probability "normalizes" the inputs to CA1 so that all synapses can contribute to CA1 firing, an assumption commonly made, but never documented, in most conceptual and computational models of the CA3-CA1 pathway.

It has been suggested that some of the memory acquisition and consolidation mechanisms could be partly understood through the study of rate and global remapping [42]. Our model makes two additional sets of predictions. During this type of remapping, at least two presynaptic features can affect the firing rate of a CA1 cell during place field traversal: the number of synapses recruited and the mean firing rate of the presynaptic cells. We showed that a differential of 75 - 125 CA3 synapses or a change by at least 1.3 Hz in CA3 firing rates were necessary for the model CA1 cell to generate significantly different firing rates (Supplemental material). Our results also show that if CA3 alone was involved in eliciting CA1 action potentials, the number of CA3 cells involved in the traversal of one CA1 place field would be about 500 ± 200. In the case of rate remapping, a redistribution of CA3 presynaptic spike trains with little change in mean firing rate (*i.e*. less than 1.3 Hz) did not result in changes in CA1 firing rate (Supplemental material). Altogether, these results suggest the existence of global and rate remapping "thresholds" bellow which the hippocampal spatial code of the animal remains relatively stable. We furthermore demonstrate that, below these thresholds, information about the remapping can potentially be carried by the precise timing of a subset of CA1 spikes ("events" in our terminology, **Figure 2**). Further experiments could test this prediction by controlling the trajectory of the animal before and after rate remapping.

Acknowledgements

We thank Stefan Leutgeb and the Moser laboratory for kindly providing the CA1 and CA3 data used in this study. Supported in part by ONR grant N000141310672, NSF CRCNS 1010172 and NSF 1117388 to JMF and a CONACYT predoctoral fellowship to NCF. Supplemental information and figures can be found of the corresponding author's website.

References

[1] Bi, G.Q. and Poo, M.M. (1998) Synaptic Modifications in Cultured Hippocampal Neurons: Dependence on Spike Timing, Synaptic Strength, and Postsynaptic Cell Type. *Journal of Neuroscience*, **18**, 10464-10472.

[2] Campanac, E. and Debanne, D. (2008) Spike Timing-Dependent Plasticity: A Learning Rule for Dendritic Integration in Rat CA1 Pyramidal Neurons. *The Journal of Physiology*, **586**, 779-793. http://dx.doi.org/10.1113/jphysiol.2007.147017

[3] Mainen, Z.F. and Sejnowski, T.J. (1995) Reliability of Spike Timing in Neocortical Neurons. *Science*, **268**, 1503-1506. http://dx.doi.org/10.1126/science.7770778

[4] Fellous, J.M., Houweling, A.R., Modi, R.H., Rao, R.P., Tiesinga, P.H., *et al*. (2001) Frequency Dependence of Spike Timing Reliability in Cortical Pyramidal Cells and Interneurons. *Journal of Neurophysiology*, **85**, 1782-1787.

[5] Maurer, A.P. and McNaughton, B.L. (2007) Network and Intrinsic Cellular Mechanisms Underlying Theta Phase Precession of Hippocampal Neurons. *Trends in Neurosciences*, **30**, 325-333. http://dx.doi.org/10.1016/j.tins.2007.05.002

[6] Sutherland, G.R. and McNaughton, B. (2000) Memory Trace Reactivation in Hippocampal and Neocortical Neuronal Ensembles. *Current Opinion in Neurobiology*, **10**, 180-186. http://dx.doi.org/10.1016/S0959-4388(00)00079-9

[7] Lee, A.K. and Wilson, M.A. (2002) Memory of Sequential Experience in the Hippocampus during Slow Wave Sleep. *Neuron*, **36**, 1183-1194. http://dx.doi.org/10.1016/S0896-6273(02)01096-6

[8] Wilson, M.A. and McNaughton, B.L. (1994) Reactivation of Hippocampal Ensemble Memories during Sleep. *Science*, **265**, 676-679. http://dx.doi.org/10.1126/science.8036517

[9] Wang, H.P., Spencer, D., Fellous, J.M. and Sejnowski, T.J. (2010) Synchrony of Thalamocortical Inputs Maximizes Cortical Reliability. *Science*, **328**, 106-109. http://dx.doi.org/10.1126/science.1183108

[10] Tiesinga, P., Fellous, J.M. and Sejnowski, T.J. (2008) Regulation of Spike Timing in Visual Cortical Circuits. *Nature Reviews Neuroscience*, **9**, 97-107. http://dx.doi.org/10.1038/nrn2315

[11] Rotman, Z. and Klyachko, V.A. (2013) Role of Synaptic Dynamics and Heterogeneity in Neuronal Learning of Temporal Code. *Journal of Neurophysiology*, **110**, 2275-2286. http://dx.doi.org/10.1152/jn.00454.2013

[12] Kandaswamy, U., Deng, P.Y., Stevens, C.F. and Klyachko, V.A. (2010) The Role of Presynaptic Dynamics in Processing of Natural Spike Trains in Hippocampal Synapses. *Journal of Neuroscience*, **30**, 15904-15914. http://dx.doi.org/10.1523/JNEUROSCI.4050-10.2010

[13] Dobrunz, L.E. and Stevens, C.F. (1997) Heterogeneity of Release Probability, Facilitation, and Depletion at Central Synapses. *Neuron*, **18**, 995-1008. http://dx.doi.org/10.1016/S0896-6273(00)80338-4

[14] Allen, C. and Stevens, C.F. (1994) An Evaluation of Causes for Unreliability of Synaptic Transmission. *Proceedings of the National Academy of Sciences of the USA*, **91**, 10380-10383. http://dx.doi.org/10.1073/pnas.91.22.10380

[15] Dobrunz, L.E., Huang, E.P. and Stevens, C.F. (1997) Very Short-Term Plasticity in Hippocampal Synapses. *Proceedings of the National Academy of Sciences of the USA*, **94**, 14843-14847. http://dx.doi.org/10.1073/pnas.94.26.14843

[16] Alabi, A.A. and Tsien, R.W. (2012) Synaptic Vesicle Pools and Dynamics. *Cold Spring Harbor Perspectives in Biology*, **4**, Article ID: a013680. http://dx.doi.org/10.1101/cshperspect.a013680

[17] Hines, M.L. and Carnevale, N.T. (1997) The NEURON Simulation Environment. *Neural Computation*, **9**, 1179-1209. http://dx.doi.org/10.1162/neco.1997.9.6.1179

[18] Major, G., Larkman, A.U., Jonas, P., Sakmann, B. and Jack, J.J. (1994) Detailed Passive Cable Models of Whole-Cell Recorded CA3 Pyramidal Neurons in Rat Hippocampal Slices. *Journal of Neuroscience*, **14**, 4613-4638.

[19] Stuart, G., Spruston, N. and Hausser, M. (1999) Dendrites. Oxford University Press, Oxford, 376 p.

[20] Cash, S. and Yuste, R. (1999) Linear Summation of Excitatory Inputs by CA1 Pyramidal Neurons. *Neuron*, **22**, 383-394. http://dx.doi.org/10.1016/S0896-6273(00)81098-3

[21] Volman, V., Levine, H., Ben-Jacob, E. and Sejnowski, T.J. (2009) Locally Balanced Dendritic Integration by Short-Term Synaptic Plasticity and Active Dendritic Conductances. *Journal of Neurophysiology*, **102**, 3234-3250. http://dx.doi.org/10.1152/jn.00260.2009

[22] Huang, E.P. and Stevens, C.F. (1997) Estimating the Distribution of Synaptic Reliabilities. *Journal of Neurophysiology*, **78**, 2870-2880.

[23] Zucker, R.S. and Regehr, W.G. (2002) Short-Term Synaptic Plasticity. *Annual Review of Physiology*, **64**, 355-405. http://dx.doi.org/10.1146/annurev.physiol.64.092501.114547

[24] Maass, W. and Zador, A.M. (1999) Dynamic Stochastic Synapses as Computational Units. *Neural Computation*, **11**, 903-917. http://dx.doi.org/10.1162/089976699300016494

[25] Matveev, V. and Wang, X.J. (2000) Differential Short-Term Synaptic Plasticity and Transmission of Complex Spike Trains: To Depress or to Facilitate? *Cerebral Cortex*, **10**, 1143-1153. http://dx.doi.org/10.1093/cercor/10.11.1143

[26] Hanse, E. and Gustafsson, B. (2001) Quantal Variability at Glutamatergic Synapses in Area CA1 of the Rat Neonatal Hippocampus. *Journal of Physiology*, **531**, 467-480. http://dx.doi.org/10.1111/j.1469-7793.2001.0467i.x

[27] Chen, G., Harata, N.C. and Tsien, R.W. (2004) Paired-Pulse Depression of Unitary Quantal Amplitude at Single Hippocampal Synapses. *Proceedings of the National Academy of Sciences of the USA*, **101**, 1063-1068. http://dx.doi.org/10.1073/pnas.0307149101

[28] Hanse, E. and Gustafsson, B. (2001) Factors Explaining Heterogeneity in Short-Term Synaptic Dynamics of Hippocampal Glutamatergic Synapses in the Neonatal Rat. *Journal of Physiology*, **537**, 141-149. http://dx.doi.org/10.1111/j.1469-7793.2001.0141k.x

[29] Dittman, J.S., Kreitzer, A.C. and Regehr, W.G. (2000) Interplay between Facilitation, Depression, and Residual Calcium at Three Presynaptic Terminals. *Journal of Neuroscience*, **20**, 1374-1385.

[30] Sun, H.Y., Lyons, S.A. and Dobrunz, L.E. (2005) Mechanisms of Target-Cell Specific Short-Term Plasticity at Schaffer Collateral Synapses onto Interneurones versus Pyramidal Cells in Juvenile Rats. *Journal of Physiology*, **568**, 815-840. http://dx.doi.org/10.1113/jphysiol.2005.093948

[31] Matveev, V. and Wang, X.J. (2000) Implications of All-or-None Synaptic Transmission and Short-Term Depression beyond Vesicle Depletion: A Computational Study. *Journal of Neuroscience*, **20**, 1575-1588.

[32] Dobrunz, L.E. and Stevens, C.F. (1999) Response of Hippocampal Synapses to Natural Stimulation Patterns. *Neuron*, **22**, 157-166. http://dx.doi.org/10.1016/S0896-6273(00)80687-X

[33] Klyachko, V.A. and Stevens, C.F. (2006) Temperature-Dependent Shift of Balance among the Components of Short-Term Plasticity in Hippocampal Synapses. *Journal of Neuroscience*, **26**, 6945-6957. http://dx.doi.org/10.1523/JNEUROSCI.1382-06.2006

[34] Markram, H., Wang, Y. and Tsodyks, M. (1998) Differential Signaling via the Same Axon of Neocortical Pyramidal Neurons. *Proceedings of the National Academy of Sciences of the USA*, **95**, 5323-5328. http://dx.doi.org/10.1073/pnas.95.9.5323

[35] Gandhi, S.P. and Stevens, C.F. (2003) Three Modes of Synaptic Vesicular Recycling Revealed by Single-Vesicle Imaging. *Nature*, **423**, 607-613. http://dx.doi.org/10.1038/nature01677

[36] Murthy, V.N., Sejnowski, T.J. and Stevens, C.F. (1997) Heterogeneous Release Properties of Visualized Individual Hippocampal Synapses. *Neuron*, **18**, 599-612. http://dx.doi.org/10.1016/S0896-6273(00)80301-3

[37] Destexhe, A., Mainen, Z.F. and Sejnowski, T.J. (1996) Kinetic Models of Synaptic Transmission. In: Koch, C., Segev, I., Eds., *Methods in Neuronal Modeling*, MIT Press, Cambridge.

[38] Wilson, M.A. and McNaughton, B.L. (1993) Dynamics of the Hippocampal Ensemble Code for Space. *Science*, **261**, 1055-1058. http://dx.doi.org/10.1126/science.8351520

[39] Destexhe, A., Rudolph, M., Fellous, J.M. and Sejnowski, T.J. (2001) Fluctuating Synaptic Conductances Recreate *in Vivo*-Like Activity in Neocortical Neurons. *Neuroscience*, **107**, 13-24. http://dx.doi.org/10.1016/S0306-4522(01)00344-X

[40] Fellous, J.M., Rudolph, M., Destexhe, A. and Sejnowski, T.J. (2003) Synaptic Background Noise Controls the Input/Output Characteristics of Single Cells in an *in Vitro* Model of *in Vivo* Activity. *Neuroscience*, **122**, 811-829. http://dx.doi.org/10.1016/j.neuroscience.2003.08.027

[41] Leutgeb, S., Leutgeb, J.K., Treves, A., Moser, M.B. and Moser. E.I. (2004) Distinct Ensemble Codes in Hippocampal Areas CA3 and CA1. *Science*, **305**, 1295-1298. http://dx.doi.org/10.1126/science.1100265

[42] Colgin, L.L., Moser, E.I. and Moser, M.B. (2008) Understanding Memory through Hippocampal Remapping. *Trends in Neurosciences*, **31**, 469-477. http://dx.doi.org/10.1016/j.tins.2008.06.008

[43] Leutgeb, S., Leutgeb, J.K., Moser, E.I. and Moser, M.B. (2006) Fast Rate Coding in Hippocampal CA3 Cell Ensembles. *Hippocampus*, **16**, 765-774. http://dx.doi.org/10.1002/hipo.20201

[44] Fenton, A.A. and Muller, R.U. (1998) Place Cell Discharge Is Extremely Variable during Individual Passes of the Rat through the Firing Field. *Proceedings of the National Academy of Sciences of the USA*, **95**, 3182-3187. http://dx.doi.org/10.1073/pnas.95.6.3182

[45] Thomson, A.M. (2000) Molecular Frequency Filters at Central Synapses. *Progress in Neurobiology*, **62**, 159-196. http://dx.doi.org/10.1016/S0301-0082(00)00008-3

[46] Abbott, L.F., Varela, J.A., Sen, K. and Nelson, S.B. (1997) Synaptic Depression and Cortical Gain Control. *Science*, **275**, 220-224. http://dx.doi.org/10.1126/science.275.5297.221

[47] Rothman, J.S., Cathala, L., Steuber, V. and Silver, R.A. (2009) Synaptic Depression Enables Neuronal Gain Control. *Nature*, **457**, 1015-1018. http://dx.doi.org/10.1038/nature07604

[48] Manor, Y. and Nadim, F. (2001) Synaptic Depression Mediates Bistability in Neuronal Networks with Recurrent Inhibitory Connectivity. *Journal of Neuroscience*, **21**, 9460-9470.

[49] Markram, H., Pikus, D., Gupta, A. and Tsodyks, M. (1998) Potential for Multiple Mechanisms, Phenomena and Algorithms for Synaptic Plasticity at Single Synapses. *Neuropharmacology*, **37**, 489-500. http://dx.doi.org/10.1016/S0028-3908(98)00049-5

[50] Goldman, M.S. (2004) Enhancement of Information Transmission Efficiency by Synaptic Failures. *Neural Computation*, **16**, 1137-1162. http://dx.doi.org/10.1162/089976604773717568

[51] Goldman, M.S., Maldonado, P. and Abbott, L.F. (2002) Redundancy Reduction and Sustained Firing with Stochastic Depressing Synapses. *Journal of Neuroscience*, **22**, 584-591.

Appendix

http://amygdala.psychdept.arizona.edu/Publications.html

Reliability and precision are optimal for non-uniform distributions of presynaptic release probability

[1,2] Jean-Marc Fellous

[1] Nadia Corral-Frías

Material and Methods – Supporting Information and Figures

Methods for Figure 1

To illustrate the consequence of recruiting high or low probability synapses on the output of a cell, we use a simple single compartment model. The neuron is contacted by 500 AMPA/NMDA synapses (see below) subdivided in two groups. The first group contains 470 synapses and is labeled 'background' the second group contains 30 synapses (6.4%, arbitrary here) and is labeled 'signal'. The background synapses receive random 5Hz Poisson presynaptic trains throughout the 500 ms simulation and each of the signal synapses receive one presynaptic input 'signal' at time 250 ms ± 10ms mimicking an input volley of 30 presynaptic spikes arriving within 20 ms of each other. All synapses have the same conductance, and are on the same compartment, so have the same elementary Excitatory Post Synaptic Potential (EPSP) if they release. The probability of these two family of synapses is uniformly fixed to either high (p=0.65) or low (0.25) values in four sets of simulations. To assess the response of the cell, the simulation is run 50 times, with the same set of presynaptic background and signal spikes and the response of the cell is plotted in a rastergram. To quantify the ability of the cell to respond to the signal, the signal to noise ratio (SNR) is computed as the number of spikes emitted between 240 ms and 275 ms (accounting for the membrane time constant of the cell, which is 10 ms, gray areas in Fig 1) divided by the total number of spikes produced.

Morphology

We used a reconstructed multi-compartmental CA1 cell from the Duke/Southampton cell archive (cell n180). This cell was chosen to represent the digitized cell population available in terms of surface area and branching structure (cells n400 and n123 were also studied with similar results, but are not discussed here for clarity). The cell membrane area was 74,686 μm^2, and contained about 600 compartments (Figure 2B). The cell surface was corrected to account for spines [1].

Cell physiology

All compartments had an axial resistance of 100 Ωcm. The compartment capacitance was increased from the standard 1 $\mu F/cm^2$ to 1.6 $\mu F/cm^2$ to account for the presence of spines [2]. In all simulations, the dendritic tree had a sigmoidal distribution of leak conductance so that distal dendritic compartments were more 'leaky' than proximal

compartments, in agreement with data collected *in vitro* in neocortex [2]. Similar experiments in hippocampus were not available. The biophysical origin of this leak is unknown, but is likely to be the result of various dendritic currents active near rest. Somatic R_m was set to 34,000 Ωcm^2 (R_{soma}) and the most distal compartment had an R_m of 5,000 Ωcm^2 (R_{end}). The half point of the sigmoid distribution was set to 400 μm and its steepness was set to 50 μm [2]. At a distance *d* from the soma, the membrane resistance was given by;

$$R_m(d) = R_{end} + \frac{R_{soma} - R_{end}}{1 - e^{\frac{400-d}{50}}} \qquad (1)$$

Active currents were located at the soma and consisted in a fast sodium current and a delayed rectifier potassium current with dynamics and conductances as in previous work [3]. A muscarinic potassium current was added to model spike frequency adaptation and adjust the cell threshold. The kinetics and conductance for this current were set as in other modeling studies [4,5]. Under these conditions, the input resistance measured at the soma by 200 pA hyperpolarizing pulses was about 60 MΩ, and the membrane time constant was about 20 ms. The resting membrane potential was kept between -70 mV and -65 mV. The voltage and current thresholds for action potential generation were about -53 mV and 500 pA respectively. These values are compatible with experimental data obtained in the hippocampal slice [6,7].

The membrane characteristics of a CA1 cell in the behaving animal are unknown. In the anesthetized preparation, CA1 resting membrane potential fluctuates around -62 mV (± 4mV) with an input resistance of about 50 MΩ, and a threshold at about -49 mV [8,9]. We further adjusted the reversal potential of the leak current to set the average membrane potential to -62 mV (the new value of this reversal potential was -55 mV). Under these conditions, the membrane potential of the CA1 cell fluctuated with a standard deviation of 3.9 mV, and its input resistance was 48 MΩ.

Model of stochastic release:

The probability of release of a single synapse was given by the equation

$$P_r(t) = 1 - e^{-F(t)/D(t)} \qquad (2)$$

where F and D are time-dependent variables representing facilitation and depression, respectively. At each excitatory synapse, when a presynaptic spike is received at time t, a random number from a uniform distribution is drawn and the probability of release, $P_r(t)$, is calculated based on the current release history S (the subset of presynaptic spike times at which the synapse has indeed released). If the random number is larger than $P_r(t)$, a postsynaptic potential is generated, and S is updated. Note that it is not necessary to update $P_r(t)$ for each synapse at every simulation time increment but only when a presynaptic spike occurs at that synapse.

$$F(t) = F_0 + \sum_{t_i < t} f(t - t_i) \text{ and } f(x) = F_{mag} e^{-x/\tau} \qquad (3)$$

F(t) is akin to an exponentially decaying accumulation of calcium with each presynaptic spike time t_i (F_0, F_{mag} and τ are constants).

$$D(t) = D_0 + \sum_{t_i < t, t_i \in S} d(t - t_i) \text{ and } d(x) = D_{mag} e^{-x/\tau'} \qquad (4)$$

where S is the dynamically updated set of spike times that yielded release (D_0, D_{mag}, τ' are constants).

The initial probability of release is therefore given by:

$$p_0 = 1 - e^{-F0/D0} \qquad (5)$$

Because F(t) and D(t) have arbitrary units, we choose D_0=1. Therefore p_0 is determined by F_0. We note that biophysically, p_0 depends on the size of the releasable vesicle pool, and the probability of release of a single vesicle. We do not expand p_0 here in terms of these factors. The parameters, F_0, F_{mag} and D_{mag} are therefore in units of D_0.

Depression:

Time constant of depression:

Depression is the result of vesicle depletion and a reduction in synaptic vesicle release probability. We aggregate these two phenomena here and show that this simplification is not detrimental to the match of the model to data. Depression is expressed as an instantaneous decrease in release probability (D_{mag}) only if the synapse has released. This condition constitutes a fundamental difference with all 'average' models that compute and use average probability, because, in our case, depression occurs only in response to a subset of the presynaptic spikes (unlike facilitation, which occurs at every presynaptic spikes). After release, the decrease in probability slowly recovers with time constant τ'. This time constant is typically slow (2-20s time scales) [10]. Because we limit our simulations to times scales compatible with that of a rat traversing a place field (2-3 sec, at normal speeds), we set this value to 2.5 seconds. Larger values did not significantly change the results presented here (tested for 5 and 10 sec, not shown).

Magnitude of depression

In order to adjust the magnitude of depression D_{mag}, we use 100 trials of 24 presynaptic pulse trains at 10 Hz, as in experiments [10]. In single CA1 synapses, synaptic depression in response to this stimulation protocol has time constants varying from 220 ms to 490 ms, depending on the amount of facilitation present, and is in the 300 ms to 400 ms range in synapses with no facilitation [10]. Because these experiments were conducted in high [Ca]/[Mg] ratios, the actual depression time constant at single synapse is expected to be somewhat larger. Unfortunately no quantitative (average) data were provided in this work. Using equations 2-5, setting F_{mag} to 0 (no facilitation), and using a distribution of F_0 yielding $N(p_0)$ as in Fig 2A, D_{mag} is completely constrained by the experimental data from synapses that do not show facilitation. Figure S1A shows the results of the simulations.

For synapses with high initial release probability, D_{mag} was found to be about 1 (in units of D_0) and the decay time constant of depression was 510 ms, compatible with experimental data (Figure S1A). The use of lower initial probability synapses increased this time constant (e.g. if p_0=0.5 the depression decay time constant was 900 ms). With lower probabilities (<0.4), the variability of responses significantly decreased the quality of the exponential fit, and the estimation of the time constant became unreliable.

Validation: In imaging experiments, paired pulse stimulation of cultured single synapses in 3mM-Ca/1mM-Mg showed that facilitation was abolished, and only synaptic depression remained [11]. Depression was found to have two components: a decrease in quantal size, and a decrease in probability of release. While a decrease in quantal size was not observed in the acute experiments of [10], our model, as tuned, should capture the decrease in probability measured by those imaging experiments. We ran simulations of synapses with various initial release probability, with facilitation blocked, stimulated by two pulses 50 ms apart, as in the experiments [11]. Figure S1B shows that, without further parameter tuning, the model exhibited a linear relationship between the probability of release during the first pulse (p_0, initial probability of release), and probability of release during the second pulse. The slope of the linear fit was 0.75, each point representing the average of 200 paired pulses. Three synapses from the imaging experiments for which these probabilities were given are plotted (open circles) and fall well within the predictions generated by the model.

Facilitation:

Time constant of facilitation:

At most CA3-CA1 synapses, facilitation has two temporal components with time constants of about 40 ms and 400 ms. As noted in other work, these two components are often well fitted by a single exponential decay function [12]. We choose here τ=120 ms, compatible with recordings made in hippocampus ([13], fitted from their Figure 1). This time constant is comparable to others obtained *in vitro* in cortex (94 -242 ms [14]), and used in other models (cortex, medium facilitation component: 190 ms [15]).

Magnitude of facilitation

Experimental evidence suggests that the magnitude of facilitation depends on the initial probability of release [16]. Our mathematical expressions (eqs 2-5) are amenable to a formal analytical derivation of this dependence.

Paired-pulse facilitation: Analytical derivation

For both a 40 ms inter-pulse interval [10] and a 50 ms interval [17], the probability of release at the time of the second pulse p_2 is well described by

$$p_2 = 1-(1-p_0)^{\frac{1}{\sqrt{p_0}}} \qquad (6)$$

In these experiments, p_2 resulted presumably from an interaction between facilitation and depression. Using our formulation (Equation (2-5)), we have therefore:

$p_2 = (1-p_0)(1-e^{-F/D_0}) + p_0(1-e^{-F/D_1})$ with

$F = F_0 + F_{mag}e^{-\frac{\Delta t}{\tau}}$ and $D_1 = D_0 + D_{mag}e^{-\frac{\Delta t}{\tau'}}$ if the synapse has released on the first pulse, and $D_1=D_0$ otherwise.

With Δt=50 ms, τ=120 ms, τ'=2500 ms, D_0=1, D_{mag}=1 and F_0=-log(1-p_0). F_{mag} is therefore a completely constrained function of p_0.Using the equations above we therefore have:

$$(1-p_0)^{\frac{1}{\sqrt{p_0}}} = (1-p_0)e^{-F/D_0} + p_0 e^{-F/D_1} \qquad (7)$$

Under the assumption that p_0 is small, the synapse is unlikely to have released on the first pulse, if p_0 is large (close to 1) the synapse is likely to have released on the 1st pulse, the equation can be simplified to:

$$F_{mag} = -A\frac{\log(1-p_0)}{\sqrt{p_0}} + B \qquad (8)$$

where A and B are constants.

The values of the constants A and B were determined from simulations. For p_0<0.5, A=-1.03, B=0.00546, for p_0>0.5 A=-1.52 and B=-0.38.

Minimal stimulation [10,18] and *in vitro* imaging experiments [17] demonstrated that the amount of paired pulse facilitation was inversely related to the initial release probability of a synapse. In our simulations, the ratio between the probability of release at the second pulse to the initial probability of release P_0 was about 2 for low reliability synapses (P_0=0.1) and 1 for reliable synapses (P_0=1).

Validation: Fixing all parameters as above, we use the analytical expression of the probability of release on two consecutive pulses and hence of paired pulse facilitation (PPF). Figure S1C shows the average ratio over 20 PPF trials for 5000 synaptic locations (error bars)(green, Equation 8). For comparison, data obtained *in vitro* are plotted on the same graph (circles) [10]. The behavior of the model is well within the variability of observed experimental data. Note that the standard errors of the simulations generally decrease as initial release probability increases, qualitatively matching the experimental data. Note also that the data were obtained from different cells, in different slices, and that therefore variability is expected to be somewhat higher than that of the model. Equation (8) is therefore a good fit to the data, and F_{mag} is completely and uniquely determined by p_0.

In sum, each individual synapse had five parameters: The unitary conductance, the initial amount of facilitation and depression (F_0 and D_0 respectively), the amount of facilitation produced by a single presynaptic action potential (F_{mag}), and the amount of depression resulting from a single release (D_{mag}).

Synaptic conductances.

AMPA: Experimental work *in vitro* shows AMPA EPSC amplitude (measured by voltage clamp at -60mV at the soma, inhibitory neurotransmission blocked) was about 14 pA when putative single synapses were stimulated [10,13]. This value is compatible with recordings from isolated synaptic boutton stimulation [11] and other hippocampal minimal stimulation data (AMPA EPSCs: 15.8 ± 7.6 pA at -80 mV [19]). EPSC amplitude is not correlated with the initial release probability of the synapse [19]. In these experiments, slices are stimulated in the stratum radiatum, activating Schaffer collaterals that make contacts on the part of the CA1 dendritic arbor that is in that stratum (main trunk and secondary branches, Figure 2B, dashed lines).

NMDA: The contribution of NMDA currents to EPSCs is highly variable from synapses to synapse. AMPA and NMDA EPSCs probabilities were experimentally found to be identical at the same synapses [19]. A proper quantification of the amount of NMDA current is complicated by the possible presence of silent synapses. We use here a NMDA/AMPA ratio of 1 to match the experimental data obtained in hippocampus CA1 of the adult rat [20].

In order to adjust the synaptic conductances in our model, we computed the average somatic EPSC resulting from the random placements of 500 single synapses in the stratum radiatum, discharging one at a time. In our passive dendritic tree models, the average of the EPSC amplitudes at -60 mV was typically equal to their standard deviation and hence followed a Poisson distribution (not shown). We found that a unitary synaptic conductance of 2.9 nS yielded an average EPSC size at the soma of 14.4 pA (± 14.5). Note that this value did not depend on the release probability of the synapse (i.e. the synapse potency is independent of initial release probability [10]). The average size of the EPSCs measured in the same compartment as the synapse was 56.0 pA (± 14.4) again compatible with data obtained from dendritic recordings [21]. The same average somatic currents could be obtained with a non-uniform distribution of AMPA channels that had a perisomatic conductance of 1.1 nS, increasing linearly (2.2 nS, 200 μm from the soma).

Validation: To further verify our tuning, we fixed all parameters, repeated the simulations above in current clamp mode (Vm at rest was set to -64 mV), and measured unitary EPSPs at the soma. The mean EPSP amplitude was 361 μV (± 329), compatible with data obtained in different experiments from connected CA3-CA1 pairs in the slice (400μV, for minimal EPSPs) [22].

At this point, all parameter values of the single synapse model have been constrained to experimental data. The only free variable remaining is the total number of synapses stimulated.

Postsynaptic synaptic currents

The dynamics of the postsynaptic AMPA current was obtained upon release using a two state kinetic scheme, NMDA channels were similarly modeled with 5 states, including desensitization and resensitization [23]. The size of the unitary EPSC measured at the soma was assumed to be constant and independent of the presynaptic stimulation patterns, compatible with single-synapse data obtained in hippocampus [24]. Short term synaptic

dynamics were found to be largely independent of the level of activation or desensitization of AMPA receptors in cortex and hippocampus [10,14,18]. Therefore, synaptic conductance and short term dynamics could be adjusted independently. There is some evidence using excised patches that AMPA synaptic conductance may increase by a factor of two to four from the perisomatic area (50 μm) to more distal locations (300 μm) [21,25,26]. Most of the data come from recordings from the main trunk, and little is known of the scaling in other dendritic areas. For comparisons, simulations were performed with synaptic conductances linearly scaled by a factor two at 200 μm from the soma. As will be indicated below, such conductance scaling had no significant impact on the conclusions presented here.

Postsynaptic macroscopic currents

To simulate the response to extracellular stimulations of the Schaffer collaterals, we distribute N synapses randomly within the stratum radiatum. This assumption is justified by the finding that when a single site is stimulated with the same stimulation pattern on two (presumably) different pathways, the responses at that site are similar [24]. This suggests that even though the synapses stimulated were different, the response remained on average the same. Hence the synaptic location was as 'random' in one pathway as it was on the other. The same stimulation pattern in a different slice (hence different CA1 neuron morphologies) would result in markedly different responses. This was successfully modeled here by substituting different cell morphologies (data not shown). The synaptic density was presumed to be constant throughout the dendritic tree, and was set to 32 synapses per 100 μm^2 of dendritic area, compatible with EM data [27]. When stimulated to mimic extracellular stimulation, all N synapses received a presynaptic spike simultaneously. This assumption is justified by the finding that the standard deviation of single synapse EPSCs latencies obtained with minimal stimulations was well below 1 ms [19].

Extracellular stimulation yields a compound EPSC at the soma, which is the result of probabilistic release at N synapses. The number of synapses activated by such stimulation is experimentally unknown. Having constrained the distribution of initial release probabilities, and the unitary conductance, we now vary the number of synapses to match the range of EPSC amplitudes measured experimentally with extracellular recordings (100-500 pA). Figure S2A shows that the average EPSC measured at the soma is a linear function of the number of synapses (each point represents the mean and standard deviation of 100 trials with a fixed number of CA3 synapses distributed randomly on the dendritic tree). The inset shows the shape of an EPSC obtained with 100 synapses. The slope of the linear fit to the data is about 2.5 (solid line). Therefore, our model predicts that an extracellular Schaffer collateral stimulation yielding 100-500 pA EPSCs at the soma is the result of the recruitment of only 25-180 synapses with release probabilities and conductances described as above. Using scaled EPSCs, the slope of the fit is 2.2 (Figure S2A, dashed line) and 25-210 synapses yield somatic amplitudes in the 100-500 pA range, not significantly different from unscaled AMPA conductances. For comparison, the figure also shows the linear fit if the distribution of initial probability is Gaussian (mean=0.28, std=0.1), and therefore does not include the high probability synapses (Figure 2C, dash-dot line). The slope of the linear fit depends on the average initial probability of the synapses and is steeper

for Gaussian distributions with higher average probability (Figure S2A: $<p_0>$= 0.5, slope = 4, $<p_0>$= 0.1, slope=1.4, data points not shown for clarity).

Validation: The variability of EPSC sizes can be measured by the coefficient of variation of EPSC amplitudes. In our simulations, it was a decreasing function of the number of synapses and could be fitted by an exponential function with a 39 synapse decay constant (Fig S2B). Experimental data obtained in slices with EPSCs measuring 204 ± 53 pA revealed EPSC variability of about 15.8% ± 3.4 [6]. According to Figure S2A, about 100 synapses (unscaled conductance) are likely to have been stimulated in these experiments to yield an EPSC average of this amplitude. The corresponding variability in our model was about 19%, compatible with the experimental findings (Figure S2B, upper arrow). This value is not significantly different from that obtained with scaled AMPA conductances (18%, not shown). Note that the model variability asymptotically approaches about 14%, a value even closer to that of the experimental data (15.8% ± 3.4). For comparison, we plot the CV of EPSC amplitudes when the initial probability distribution is Gaussian centered at the same mean as $N(p_0)$ (mean=0.28, standard deviation=0.1, Figure S2B dashed line). This distribution does not include the high probability synapses that form the tail of the experimentally derived distribution (Figure 1B). For this distribution, the CV is significantly higher and would enter the experimental range of 15.8% ± 3.4 at about 300 synapses. Figure S2A shows however that such a number of synapses would yield a somatic EPSC of about 800 pA, which is incompatible with what was obtained experimentally (204 ± 53 pA). Our model therefore suggests that a naïve, Gaussian-like distribution of initial probability cannot satisfy both the variability and the size of the somatic EPSC observed experimentally.

To complement the study of EPSC variability, and further validate our model, the variability of EPSPs measured at the soma was assessed by stimulating N synapses 50 times, and by computing the coefficient of variation of EPSP amplitudes, while the cell was slightly hyperpolarized to avoid spiking (-250 pA, as in experiments). The CV was a decreasing function of N that could be well fitted by an exponential function with a decay constant of 46 synapses. To compare with data, using the assumption above that about 100 synapses were stimulated, our simulations show that the EPSP variability is about 13%, (S2B, lower arrow) again, compatible with experimental data (13.7% ± 3%) [6]. This value is not significantly different from that obtained with scaled AMPA conductances (16%, not shown). Again, the model asymptotically converges close to the value observed experimentally.

Taken together, these modeling results suggest that most extracellular stimulations of the Schaffer collaterals *in vitro* recruit a low number of synapses in the range of 100 or less, and that a skewed distribution of initial release probability (Figure 2A) is required to account for both the variability and the size of the postsynaptic currents observed experimentally *in vitro*.

Input spike trains

The inputs spike trains to our model CA1 cell were taken from a population of 37 CA3 pyramidal cells recorded simultaneously in four 10 minutes sessions, as the animal was exploring a rectangular box [28]. For each cell, place

fields were characterized using video tracking data (single place fields). Each traversal of each place field of each cell was isolated, and the corresponding spike trains were collected. Figure S3A shows 300 of the 992 CA3 spike trains thus collected. Spike trains contained all the classical characteristics of CA3 place cells, including bursts and theta modulation. For technical reasons, it is not possible to record from more than about 100 cells simultaneously. To simulate N CA3 inputs to a CA1 cell (N up to 900 here), we randomly picked from the 992 spike trains obtained by the procedure above, and made the assumption that the variability observed in randomly picking N spike trains out of 992 place field traversals of 37 CA3 cells was similar to that of N different CA3 cells recorded simultaneously as the animal traverses a single region of space only once. The inset of Figure S3A shows the distribution of CA3 mean firing rates during place field traversal (4.7 ± 4.3 Hz, computed in a 4 second window centered on the crossing of the center of the field as displayed in the rastergram). In the same manner, 1878 spike trains were collected in the same apparatus, from 26 simultaneously recorded CA1 place cells exhibiting a well defined and unique place field. These spike trains are used to assess the response of the model CA1 cell.

At least two presynaptic features can affect the firing rate of the CA1 cell in a particular environment; the number of CA1 synapses recruited during the place field traversal (number of CA3 place fields overlapping with the CA1 place field), and the mean firing rate of the presynaptic CA3 cells. A change in the population of presynaptic CA3 synapses recruited mimics the CA3 component of global remapping. A change in the firing rate of a fixed set of CA3 synapses mimics rate remapping [29].

Choosing a realistic number of input CA3 synapses

Figure S3B shows the in-field firing rate of the simulated CA1 cell for different numbers of presynaptic CA3 cells (assuming one synapse per CA3 cell). In the range of 200 to 800 synapses, the firing rate increases quasi-linearly with the number of CA3 synapses recruited. In these simulations, different sets of synapses are randomly selected for each X-axis value. Experimental CA1 cells in-field firing rates measured simultaneously with CA3 were 3.6 Hz ± 2.7Hz (2B horizontal lines). This modeling result suggests therefore that, if CA3 alone was involved in discharging CA1, the number of CA3 place cells involved in the traversal of one CA1 place field would be about 500 ± 200. Note that since CA1 also receives inputs from the entorhinal cortex, the actual number of CA3 inputs involved in discharging a given CA1 cell is likely to be smaller. A statistical analysis of the simulation results shows that a differential of 75-125 CA3 synapses is required to change the CA1 firing rate significantly (paired t-tests between consecutive points in the graph, $p<0.05$). This suggests that global remapping (change in CA3 afferent synapse population) will not affect a CA1 cell unless at least 75-125 CA3 cells remap spatially. While the exact number of synapses yielding significance depends on the number of samples and other parameters of our simulations, this result suggests that global remapping will occur only after a sufficient number of individual cells have remapped. According to this model, global remapping has a 'threshold' (here of about 75-125 cells) below which the mapping should be spatially robust.

Figure S3C shows the mean CA1 firing rate (40 trials per points) as a function of the mean firing rate of the CA3 inputs (500 fixed synapses, randomly distributed on the dendritic arbor in the stratum radiatum). The slope was 0.8 Hz/Hz. A paired t-test analysis on consecutive points indicated that a differential of about 1.3Hz in CA3 firing

rates was necessary for the CA1 cell to generate significantly different firing rates. The arrow points to the nominal CA3 mean firing rate obtained from 500 of the 992 spike trains in panel A. The inset shows a sample voltage trace from the simulated CA1 cell responding to one trial with 500 synapses. This result suggests that a rate remapping in CA3 will not be detected by CA1 unless the average firing rate in CA3 changes by more than 1.3 Hz.

These results justify our choice of 500 CA3 input synapses.

Reliability and Precision

To quantify their occurrence we use the 'direct method' for the computation of reliability and precision [30]. Briefly, a histogram is constructed from the 40-trial rastergram (15 ms bins) and smoothed (Gaussian kernel of 6 ms). A threshold is computed as 4 standard deviations away from the mean of the smoothed histogram. All threshold crossings are termed 'events' and correspond to alignments in the 40-trial rastergram. The width of each event is computed as the width of the smoothed histogram peaks at mid-height. All spike times falling within the width of any event are counted as reliable spikes. The reliability R if the fraction of all the spikes generated by CA1 that fall within a reliable event across the 40 trials ($0 \leq R \leq 1$).

The standard deviation σ_e of the spike times falling in each event is computed. This value gives an indication of the jitter with which reliable spikes are produced, for each specific event. The average jitter σ is computed across all events in the rastergram. We define the precision of the response as $P=1/2\sigma$. P is expressed in Hertz and can be interpreted as the maximal frequency at which a cell which generate spikes with a jitter of standard deviation σ when driven so that it generates only one spike in at least 50% of all the cycles (i.e. above chance). P/2 is the maximal driving frequency that would generate exactly 1 spike per cycle (the period of this frequency is 4σ, approximately the width at the base of a Gaussian distribution of standard deviation σ). Both R and P are specific to the particular CA3 presynaptic spike pattern used to obtain the 40-trial rastergram.

References cited

1. Major G, Larkman AU, Jonas P, Sakmann B, Jack JJ (1994) Detailed passive cable models of whole-cell recorded CA3 pyramidal neurons in rat hippocampal slices. J Neurosci 14: 4613-4638.
2. Stuart G, Spruston N (1998) Determinants of voltage attenuation in neocortical pyramidal neuron dendrites. J Neurosci 18: 3501-3510.
3. Traub RD, Jefferys JG, Miles R, Whittington MA, Toth K (1994) A branching dendritic model of a rodent CA3 pyramidal neurone. J Physiol 481: 79-95.
4. Yamada W, Koch C, Adams PR (1989) Multiple Channels and Calcium Dynamics. In: Koch C, Segev I, editors. Methods in Neuronal Modeling: From synapses to Networks. Cambridge, Massachusets: M.I.T. Press. pp. 97-133.
5. Gutfreund Y, Yarom Y, Segev I (1995) Subthreshold oscillations and resonant frequency in guinea-pig cortical neurons: physiology and modelling. J Physiol (Lond) 483: 621-640.
6. Otmakhov N, Shirke AM, Malinow R (1993) Measuring the impact of probabilistic transmission on neuronal output. Neuron 10: 1101-1111.
7. Altemus KL, Lavenex P, Ishizuka N, Amaral DG (2005) Morphological characteristics and electrophysiological properties of CA1 pyramidal neurons in macaque monkeys. Neuroscience 136: 741-756.

8. Henze DA, Buzsaki G (2001) Action potential threshold of hippocampal pyramidal cells in vivo is increased by recent spiking activity. Neuroscience 105: 121-130.
9. Isomura Y, Sirota A, Ozen S, Montgomery S, Mizuseki K, et al. (2006) Integration and segregation of activity in entorhinal-hippocampal subregions by neocortical slow oscillations. Neuron 52: 871-882.
10. Dobrunz LE, Stevens CF (1997) Heterogeneity of release probability, facilitation, and depletion at central synapses. Neuron 18: 995-1008.
11. Chen G, Harata NC, Tsien RW (2004) Paired-pulse depression of unitary quantal amplitude at single hippocampal synapses. Proc Natl Acad Sci U S A 101: 1063-1068.
12. Zucker RS, Regehr WG (2002) Short-term synaptic plasticity. Annu Rev Physiol 64: 355-405.
13. Dobrunz LE, Huang EP, Stevens CF (1997) Very short-term plasticity in hippocampal synapses. Proc Natl Acad Sci U S A 94: 14843-14847.
14. Varela JA, Sen K, Gibson J, Fost J, Abbott LF, et al. (1997) A quantitative description of short-term plasticity at excitatory synapses in layer 2/3 of rat primary visual cortex. J Neurosci 17: 7926-7940.
15. Matveev V, Wang XJ (2000) Differential short-term synaptic plasticity and transmission of complex spike trains: to depress or to facilitate? Cereb Cortex 10: 1143-1153.
16. Thomson AM (2000) Facilitation, augmentation and potentiation at central synapses. Trends Neurosci 23: 305-312.
17. Murthy VN, Sejnowski TJ, Stevens CF (1997) Heterogeneous release properties of visualized individual hippocampal synapses. Neuron 18: 599-612.
18. Hanse E, Gustafsson B (2001) Factors explaining heterogeneity in short-term synaptic dynamics of hippocampal glutamatergic synapses in the neonatal rat. J Physiol 537: 141-149.
19. Hanse E, Gustafsson B (2001) Quantal variability at glutamatergic synapses in area CA1 of the rat neonatal hippocampus. J Physiol 531: 467-480.
20. Hestrin S, Nicoll RA, Perkel DJ, Sah P (1990) Analysis of excitatory synaptic action in pyramidal cells using whole-cell recording from rat hippocampal slices. J Physiol 422: 203-225.
21. Smith MA, Ellis-Davies GC, Magee JC (2003) Mechanism of the distance-dependent scaling of Schaffer collateral synapses in rat CA1 pyramidal neurons. J Physiol 548: 245-258.
22. Sayer RJ, Friedlander MJ, Redman SJ (1990) The time course and amplitude of EPSPs evoked at synapses between pairs of CA3/CA1 neurons in the hippocampal slice. J Neurosci 10: 826-836.
23. Destexhe A, Mainen ZF, Sejnowski TJ (1996) Kinetic models of synaptic transmission. In: Koch C, Segev I, editors. Methods in neuronal modeling. Cambridge: M.I.T. Press.
24. Dobrunz LE, Stevens CF (1999) Response of hippocampal synapses to natural stimulation patterns. Neuron 22: 157-166.
25. Andrasfalvy BK, Magee JC (2001) Distance-dependent increase in AMPA receptor number in the dendrites of adult hippocampal CA1 pyramidal neurons. J Neurosci 21: 9151-9159.
26. Magee JC, Cook EP (2000) Somatic EPSP amplitude is independent of synapse location in hippocampal pyramidal neurons. Nat Neurosci 3: 895-903.
27. Harris KM, Jensen FE, Tsao B (1992) Three-dimensional structure of dendritic spines and synapses in rat hippocampus (CA1) at postnatal day 15 and adult ages: implications for the maturation of synaptic physiology and long-term potentiation. J Neurosci 12: 2685-2705.
28. Leutgeb S, Leutgeb JK, Treves A, Moser MB, Moser EI (2004) Distinct ensemble codes in hippocampal areas CA3 and CA1. Science 305: 1295-1298.
29. Colgin LL, Moser EI, Moser MB (2008) Understanding memory through hippocampal remapping. Trends Neurosci.
30. Tiesinga P, Fellous JM, Sejnowski TJ (2008) Regulation of spike timing in visual cortical circuits. Nat Rev Neurosci 9: 97-107.

Supplemental Figures

Figure S1: Tuning and validation of synaptic parameters. A: Somatic EPSC amplitude in response to a train of 24 pulses at 10Hz. The exponential fit (red curve) gives a time constant of 510 ms. B: Validation of the synaptic

parameters of depression: After the tuning achieved in A, all other parameters fixed, the model was run on a new experimental paradigm: Paired pulse (50 ms ISI) protocol for synapses with various initial probability of release. Red circle are from actual data (Chen et al. 2004). C: Validation of the synaptic parameters for facilitation. Pair-pulse facilitation ratio (50 ms ISI) is plotted as a function of initial release probability. Points with error bars: simulation data showing the average and standard deviation of the PPF ratio computed at 5000 locations in the dendritic tree, each averaged across 20 trials. Circles: Data from Dobrunz et al. (1997). Continuous curve: Continuous fit (eq 6) from Dobrunz et al. (1997).

Figure S2: Tuning and validation of postsynaptic currents. A: Somatic EPSC as a function of the number of CA3 synapses stimulated. Circles and error bars: simulation data (100 trials). Dashed line indicate EPSC size typically recorded experimentally (100-500 pA) suggesting a recruitment of 25-180 synapses. Solid line is the linear fit. Dash-dot line is the linear fit for a Gaussian distribution of initial release probability centered at 0.28 ± 0.1, data points not shown for clarity). Dashed line is the linear fit for scaled AMPA conductances. Two other solid lines are fits for Gaussian distributions of initial probabilities centered at 0.5 and 0.1 (data points not shown for clarity). B: Validation of the tuning in A. Coefficient of variation of EPSP (positive values) and EPSC (negative values) plotted on the same graph, as a function of the number of synapses stimulated. Arrows point to values measured experimentally by Otmakhov et al. (1993): 15.8% for EPSCs and 13.7% for EPSPs. Continuous line is an exponential fit to the simulation data. Dashed line is the exponential fit when the initial probability of release is distributed as a Gaussian centered at 0.28 (with no high probability tail, data points not shown for clarity).

Figure S3: Firing during place field traversal. A: rastergram showing 300 of the 992 spike trains obtained from 37 simultaneously recorded CA3 single-place-field cells (Leutgeb et al. 2004). Spike trains were aligned at the center of their respective place fields. The inset shows the distribution of CA3 firing rates. B: Mean firing rate of the CA1 cell as a function of the number of presynaptic CA3 inputs. All CA3 synapses were stimulated with inputs randomly drawn from 2A. C: Mean firing rate of the CA1 cell in response to variations in the mean CA3 firing rate (500 synapses). The arrow point to the mean firing rate as measured in the data (random sampling from 2A). The four other points were obtained by re-sampling 500 spike trains from 2A so that the CA3 mean firing rate varied between 1 and 8 Hz. Inset: sample voltage trace of the CA1 cell stimulated by 500 synapses (arrow). Scale bar is 10 mV, 500 ms.

Supplemental figures

Figure Supp.1

A

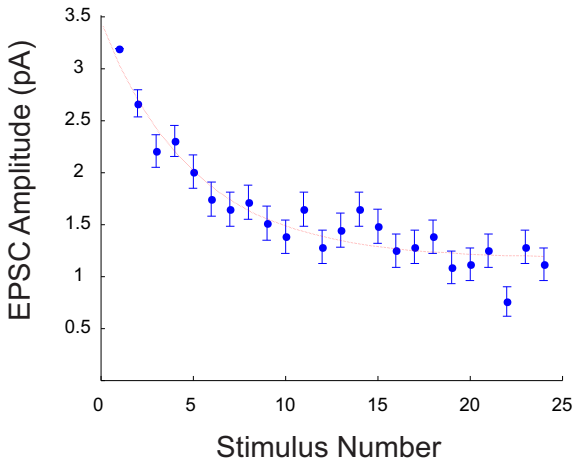

B

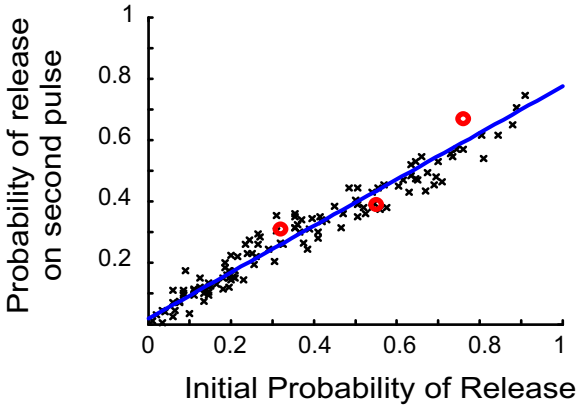

C

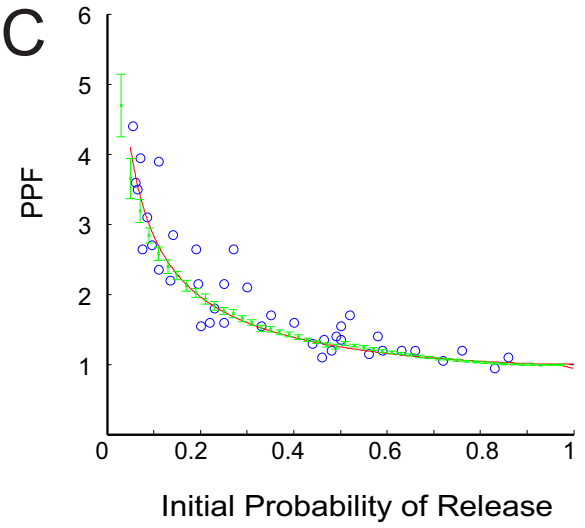

Supplemental figures

Figure Supp.2

A

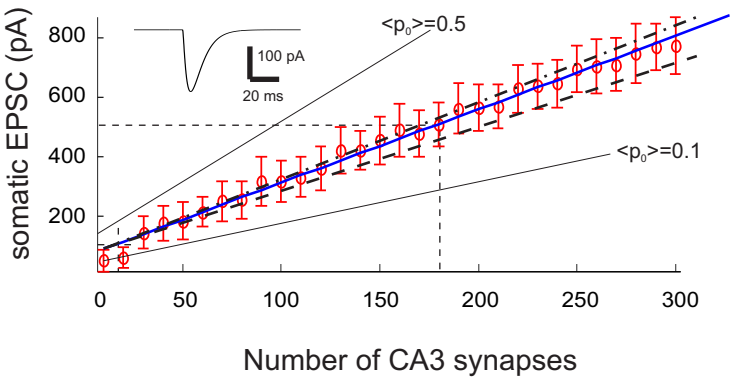

B

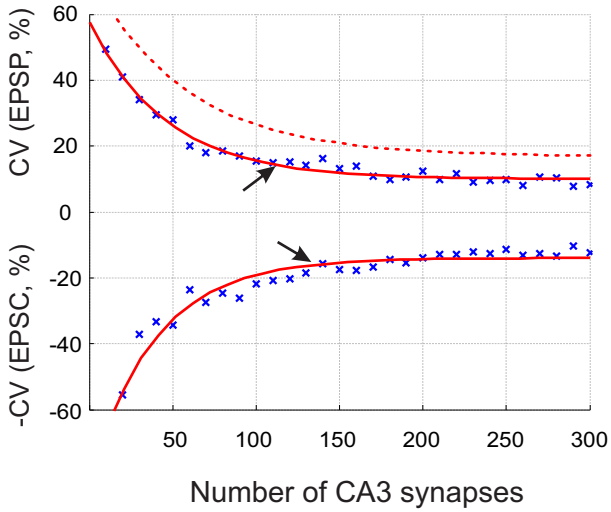

Supplemental figures
Figure Supp.3